Article

Phytochemical Curcumin-Coformulated, Silver-Decorated Melanin-like Polydopamine/Mesoporous Silica Composites with Improved Antibacterial and Chemotherapeutic Effects against Drug-Resistant Cancer Cells

Yiyan Song,[#] Ling Cai,[#] Zhongcheng Tian, Yuan Wu,* and Jin Chen*

Cite This: *ACS Omega* 2020, 5, 15083−15094

Read Online

ACCESS | Metrics & More | Article Recommendations | Supporting Information

ABSTRACT: The devastating occurrence of drug resistance such as antimicrobial resistance has aroused global concerns for public health, which has propelled a continuous pursuit of safe and effective therapeutic agents. In this study, silver nanoparticles were decorated in mesoporous silica of SBA-15 coated with melanin-like polydopamine (PDA) as nanocarriers. Meanwhile, the constructed mesopore was loaded with phytochemical curcumin (CCM) through its noncovalent interactions with PDA coatings. The obtained CCM@SBA-15/PDA/Ag composites were characterized by physicochemical methods and exhibited desirable biocompatibility and low hemolytic activity. The dual-stimuli-responsive (pH and ROS) release of curcumin and/or silver nanoparticles from the CCM@ SBA-15/PDA/Ag composites was achieved to reduce the side effects of noncontrolled drug leakage under physiological conditions. Additionally, compared with that of SBA-15/PDA/Ag and CCM@SBA-15/PDA, CCM@SBA-15/PDA/Ag combination showed a prolonged inhibitory effect on bacterial growth of G⁻ *E. coli* (72 h) and G⁺ *S. aureus* (24 h), attributing to the enhanced effect of the bactericide of silver nanoparticles and curcumin. Furthermore, through the utilization of the nanoformulation of curcumin, improved chemotherapeutic efficiency against human cervical cancer cells (HeLa) and Taxol-resistant nonsmall cell lung cells (A549/TAX) was identified in comparison with that of free curcumin. Thus, our study rationalized the combinational design of the natural compound and silver nanoparticles as an integrated dual-responsive nanoplatform in dealing with infectious bacteria and drug resistance in cancers for enhanced therapy.

1. INTRODUCTION

In recent years, the spread of drug resistance has become a global concern.[1,2] For example, the bacteria that resist antibiotics were framed as the most threatening types to the public health by the World Health Organization (WHO).[3] Meanwhile, drug-resistance phenotypes in cancer cells also existed, such as drug resistance engendered by the use of taxane and doxorubicin.[4−7] Although using a high dose of drugs may overcome drug resistance temporarily, it may in turn cause acute toxicities and accelerate the emergence of drug resistance. Thus, it is imperative to explore safe and effective agents with improved antibacterial and/or antitumor activities that may alleviate drug resistance to a great extent.

Mesoporous silica nanoparticles (MSNs) have attracted tremendous attention in drug delivery and antimicrobial application due to their great biocompatibility, easy surface functionalization, and excellent drug loading capacity. In particular, Santa Barbara Amorphous-15 (SBA-15) possesses a highly ordered hexagonal channel structure with large pore volume and good biodegradability.[8] As a drug delivery system, MSNs have been utilized to carry therapeutic drugs to the targeted location. Unlike free drugs, MSNs can accumulate and remain in tumor cells rather than rapidly metabolized.[9] Furthermore, the controlled release of the drugs from the MSN framework provides an enhanced therapeutic effect.[10,11]

Curcumin (CCM), regarded as an ancient medicine for centuries, is a natural compound extracted from the herb *Curcuma longa* rich in polyphenolic substances.[12,13] This economical and safe drug possesses broad biological functions, such as antioxidant, anti-inflammatory, anticarcinogenic, antimicrobial, and chemopreventive properties.[14−16] Notably, curcumin was capable of inhibiting the proliferation of several cancer cells due to its suppression of the activation of transcriptional factor NFκB.[17,18] More recently, it was also shown that curcumin exhibited superior synergistic effect against the wide spectrum of bacteria and cancer cells when combined with other active components like nanoparticles,
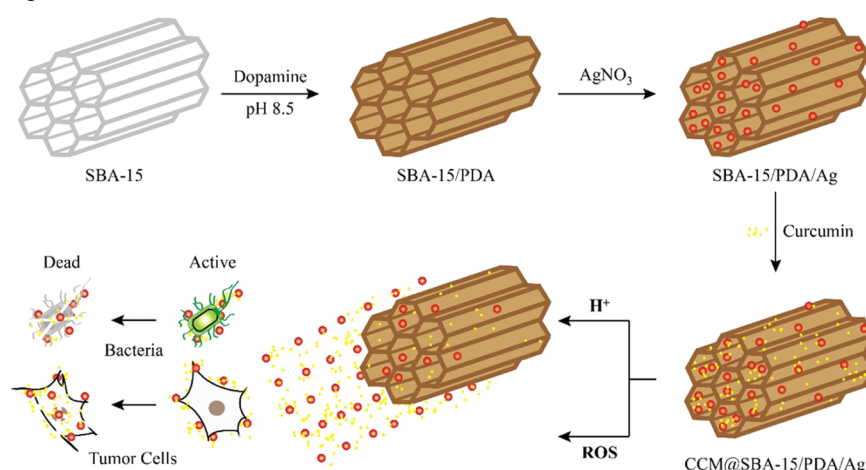
Scheme 1. Nanoformulation of SBA-15/PDA/Ag with or without the Encapsulation of Curcumin and Resulting Dual-Stimuli-Responsive Behaviors against Bacterial and Tumor Cells

antibiotics, and antitumor drugs.[4,19,20] In particular, in contrast to other pharmaceuticals, previous animal and human pharmacokinetic studies have validated the extreme safety of curcumin even at a high dose of 12 g/day.[14] Nevertheless, the practical application of curcumin was limited due to its low water solubility and poor bioavailability, which resulted in the fast metabolism and low body absorption.[12] In this regard, owing to the high stability and large surface area, ordered mesoporous silica nanoparticles that were coformulated with curcumin have demonstrated the capability to improve the aqueous solubility of curcumin with desirable stability.[21]

Melanin-like biopolymers commonly exist in the human tissues and organs including hair, skin, and brain medulla,[18] which were widely used in the fields of biosensing, diagnosis, and tissue engineering due to their superior biocompatibility and biodegradable nature.[22−27] Among melanin-like biopolymers, polydopamine (PDA) possessed remarkable interfacial reinforcement when adhered to diverse types of material surfaces due to the abundant amine and/or catechols.[28−30] PDA-based surface modification nanoplatforms have been investigated widely in the field of biomedicine due to the pH, reactive oxidative species (ROS), and near-infrared (NIR) multiresponsive properties.[8,31] Typically, nanocarriers coated with PDA are utilized for controlled drug release and photothermal therapy on tumor cells.[32,33] Under mild alkaline conditions, the aromatic hydroxyl moieties of PDA can promote the stable formation of metal nanoparticles without the addition of other reducing agents.[34−36] Furthermore, PDA with plentiful aromatic rings on the surface enabled a high payload of therapeutic molecules such as curcumin via $\pi-\pi$ stacking and/or hydrogen bonding.[37,38] The built nanoformulation of PDA layers combined with curcumin may endow the therapeutic excipients with a smart function, including the acid- and/or reactive oxidative species (ROS)-triggered release of loaded drugs, which was expected to improve the bioavailability of curcumin for the purpose of targeted and controlled therapy.

Silver nanoparticles represented promising potentials as antibacterial agents due to their low toxicity, high cost-effectiveness, and broad spectrum activity.[39] The bactericidal effect of silver nanoparticles came from their ability to increase the bacteria membrane permeability upon penetration into the cytoplasm, followed by protein denaturation and termination

of DNA replication.[40] Therefore, silver nanoparticle administration was considered as an alternative bactericide compared to other classical antibiotics, especially with the emergence of drug resistance to most current clinical regimens.[41] In addition, the use of silver nanoparticles as an antitumor nanomedicine has also been reported, which showed their promising efficacy in cancer therapy.[42,43] Nevertheless, the practical applications of silver nanoparticles are limited because of their inherent aggregation-prone tendency. The biomimetic polymers including PDA,[44,45] seaweed,[46,47] and tea polyphenol,[48] with abundant chemically active groups, provided a mild autoreduction platform to form silver nanoparticles of homogenous distribution, which showed advantageous properties for biomedical uses.

In this study, we utilized the biocompatible ordered mesoporous SBA-15 as nanocarriers for self-polymerized dopamine coating and the silver nanoparticles were in situ decorated in the composite through the reduction reaction with the PDA layer. Subsequently, curcumin was further encapsulated into the mesopores of SBA-15/PDA/Ag via $\pi-\pi$ stacking and/or hydrogen bonding between the PDA layer and curcumin (Scheme 1). Moreover, the prepared CCM@SBA-15/PDA/Ag composites exerted improved biocompatibility toward mammalian red blood cells and were characterized by physicochemical methods. Meanwhile, the highly biocompatible CCM@SBA-15/PDA/Ag composites exerted smart pH- and/or ROS-triggered curcumin and/or silver release. This mesoporous melanin-like PDA with silver nanoparticle deposition and curcumin encapsulation provided a promising and effective combination therapy to combat the growth of infectious bacteria and cancer.

2. RESULTS AND DISCUSSION

2.1. Characterization of Obtained Nanocomposites.
The preparation and utilization of SBA-15/PDA nanocomposites as the delivery matrix of curcumin and silver are illustrated in Scheme 1. The length of SBA-15 was ~1.5 μm with the typical hexagonal channel structure. The PDA film was formed by the polymerization of dopamine on the inner surface of mesopores and the outer surface of SBA-15 and the silver nanoparticles were in situ reduced and deposited on the PDA film. Finally, curcumin was loaded on the PDA layer via $\pi-\pi$ stacking and/or hydrogen bonding. As measured by
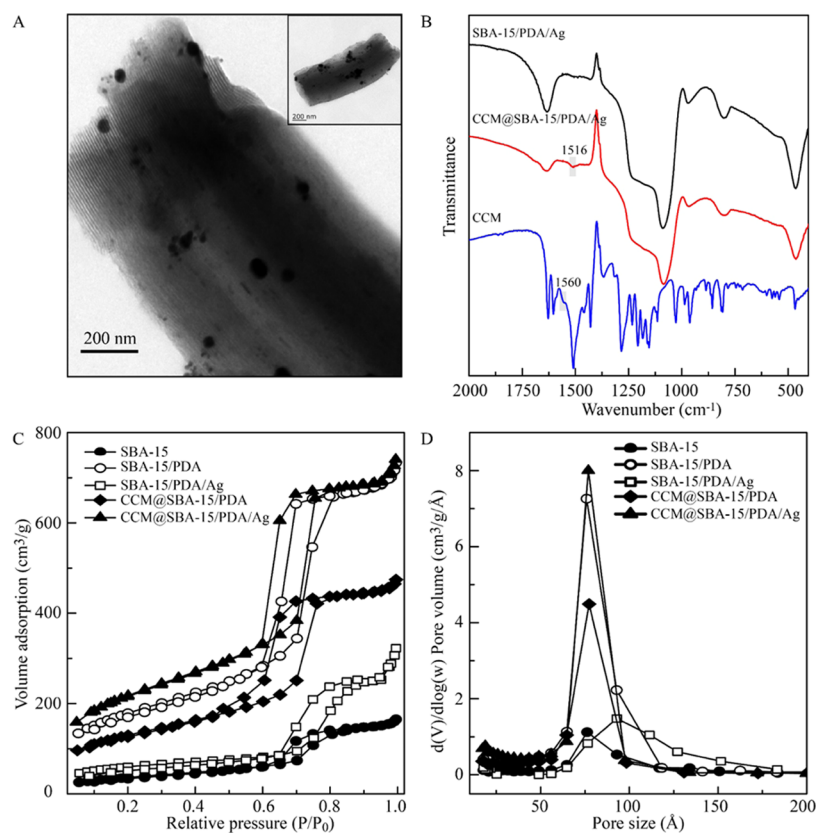
Figure 1. (A) HRTEM image of the CCM@SBA-15/PDA/Ag composite with the corresponding TEM image shown in the inset. (B) FT-IR spectra of SBA-15/PDA/Ag, CCM@SBA-15/PDA/Ag, and CCM. (C) Nitrogen adsorption−desorption isotherms of SBA-15, SBA-15/PDA, SBA-15/PDA/Ag, CCM@SBA-15/PDA, and CCM@SBA-15/PDA/Ag powders and (D) corresponding pore size distribution curves from the Barret−Joyner−Hallender (BJH) adsorption branch.

HPLC, the loading amount of curcumin was found to be 18.6 mg/g. The silver contents of SBA-15/PDA/Ag and CCM@SBA-15/PDA/Ag measured by ICP were 9.70 and 9.28%, respectively.

The morphology of the obtained composites was directly evaluated by TEM. As shown in Figure 1A, the as-prepared CCM@SBA-15/PDA/Ag retained the ordered hexagonal mesostructure of rodlike SBA-15. The silver nanoparticles were in situ formed by the reduction of coated PDA distributed on both the outer and inner surfaces of SBA-15, and the size of inner silver nanoparticles was obviously smaller than that of the outer ones. The homogeneously distributed silver nanoparticles could be observed by SEM (shown Figure S1A), which may be attributed to the positively charged PDA preventing the aggregation of silver nanoparticles by reciprocal electrostatic repulsion.[43,49−51] The elemental compositions and distributions were verified by EDS (Figure S1C) and mapping results (Figure S1B), which revealed the evident existence of C, N, O, Si, and Ag in the composite CCM@SBA-15/PDA/Ag with elements distributing uniformly.

Fourier transform infrared (FT-IR) spectra (shown in Figure 1B) were measured to validate the chemical groups formed on the nanoexcipient upon drug loading. The characteristic framework vibration region of SBA-15 consisted of bands centered at 1086, 968, and 806 cm^{-1}, respectively. The 1086 and 806 cm^{-1} peaks were assigned to Si−O asymmetric and symmetric stretching bands originating from the intrinsic vibration of SiO_4 tetrahedra, respectively.[52] The characteristic peak of curcumin at 1560 cm^{-1} was the C=O stretching

band,[21] but after loading curcumin on the nanoexcipient, the typical band was red-shifted to a lower wavenumber, indicating the involvement of carbonyl groups of curcumin in the chelation of silver and successful loading of curcumin in nanoexcipient SBA-15/PDA/Ag.

Nitrogen adsorption−desorption was performed to probe the porous structures. The isotherms of SBA-15, SBA-15/PDA, SBA-15/PDA/Ag, CCM@SBA-15/PDA, and CCM@SBA-15/PDA/Ag exhibited a type IV isotherm with a N_2 hysteresis loop (shown in Figure 1C), pointing to the existence of mesoporous structures.[53,54] Figure 1D indicated that except for SBA-15/PDA/Ag composites (78. 5375 Å), there was an obvious decrease in the pore size of obtained materials, i.e., 75.972 Å for SBA-15, 70.879 Å for SBA-15/PDA, 63.020 Å for CCM@SBA-15/PDA, and 58.804 Å for as-prepared CCM@SBA-15/PDA/Ag, suggesting the successful coating of polydopamine and high loading of curcumin in the mesopores. The enlargement of the pore size of as-prepared SBA-15/PDA/Ag compared to that of SBA-15/PDA composites may be attributed to the change in the PDA layer in the process of in situ formation of silver nanoparticles. Accordingly, the BET surface areas and pore volumes of the as-prepared materials are detailed in Table 1. The BET surface area and pore volume of SBA-15/PDA increased due to the PDA coating on the mesoporous siliceous support, while these parameters decreased for SBA-15/PDA/Ag, which accorded with our previous work.[50] These characterization results may therefore indicate a good formation of PDA coatings on SBA-15 possessing mesoscale regularity, which was favorable for the

Table 1. Mesostructural Parameters of SBA-15, SBA-15/PDA, SBA-15/PDA/Ag, CCM@SBA-15/PDA, and CCM@SBA-15/PDA/Ag

| sample	BET surface area (m^2/g)	pore volume (cm^3/g)	average pore size (Å)
SBA-15	134.356	0.255	75.972
SBA-15/PDA	640.306	1.135	70.879
SBA-15/PDA/Ag	299.844	0.5887	78. 538
CCM@ SBA-15/PDA	465.465	0.733	63.020
CCM@ SBA-15/PDA/Ag	779.322	1.146	58.804

autoreduction and deposition of $AgNO_3$ and a simultaneous efficient curcumin loading.

The small-angle XRD results (Figure S2A) showed that the ordered mesostructure of SBA-15 was maintained after the coating of the PDA film and further loading of curcumin, while such regularity was decreased after the formation of silver nanoparticles on SBA-15/PDA and the further loading of curcumin on SBA-15/PDA/Ag. These results were in good accordance with the observation of nitrogen adsorption—desorption measurements. The wide-angle XRD patterns of SBA-15, SBA-15/PDA, SBA-15/PDA/Ag, and CCM@SBA-15/PDA, and CCM@SBA-15/PDA/Ag are shown in Figure S2B. The broad reflection peaks of SBA-15, SBA-15/PDA, and CCM@SBA-15/PDA indicated the amorphous nature of the manufactured materials. For as-prepared SBA-15/PDA/Ag and CCM@SBA-15/PDA/Ag, four peaks centered at 38.139, 44.319, 64.460, and 77.400° corresponding to the Bragg reflections from (111), (200), (220), and (311) planes of Ag, respectively (JCPDS card no. 04-0783), indicate the formation of the cubic structure of metallic Ag[47] and the invariance of the crystalline of silver after curcumin loading. The other small peaks at 27.840, 32.259, 46.242, 54.838, 57.480, 67.459, 74.460, and 76.722° were characteristics of the (111), (200), (220), (311), (222), (400), (331), and (420) planes of AgCl, respectively (JCPDS card no. 06-0480), which pointed out the small amount of existing AgCl particles possibly from chloride

ions in the buffer solution during the synthesis process. The average crystallite sizes for the silver components of SBA-15/PDA/Ag and CCM@SBA-15/PDA/Ag were calculated to be 37.0 and 49.5 nm using the Scherrer formula,[55] respectively, suggesting that the presence of CCM was beneficial for the formation of silver nanoparticles.

The zeta potentials of SBA-15, SBA-15/PDA, SBA-15/PDA/Ag, and CCM@SBA-15/PDA/Ag were measured, and the results are shown in Figure S3. It was found that the zeta potential of SBA-15 was -14.2 ± 0.86 mV because of the silicon hydroxyl groups on the surface. The zeta potential of SBA-15/PDA was declined to -29.5 ± 0.55 mV due to the abundant phenolic hydroxyl groups of the PDA layer. After the subsequent incorporation of silver nanoparticels into the composites, the zeta potential was increased to 0.448 ± 0.42 mV, which indicated that the silver nanoparticles were positively charged in the SBA-15/PDA/Ag composites. Finally, the zeta potential of CCM@SBA-15/PDA/Ag was -18.9 ± 0.666 mV, which was attributed to the phenolic hydroxyl groups of curcumin, suggesting the successful loading of curcumin molecules.

2.2. Biocompatibility Evaluation of Materials. The biocompatibility of the nanotheranostic excipient is the major concern for clinical applications. To this end, the toxic effect of the manufactured samples on mammalian cells, especially red blood cells (RBCs), was evaluated by measuring the hemolytic behavior of cells exposed to different concentrations of samples ranging from 31 to 500 μg/mL. As shown in Figure 2, there was no obvious hemolytic activity identified in the presence of SBA-15/PDA and CCM@SBA-15/PDA at a high concentration up to 500 μg/mL, demonstrating the desirable biocompatibility of SBA-15/PDA and CCM@SBA-15/PDA with RBCs. After the in situ formation of silver nanoparticles in the mesopores of SBA-15/PDA composites, the percentage of hemolysis at the concentration of 500 μg/mL SBA-15/PDA/Ag is ~45% compared with control groups ($P < 0.05$, there were statistically significant differences between SBA-15/PDA/Ag-treated groups and control groups), while no evident
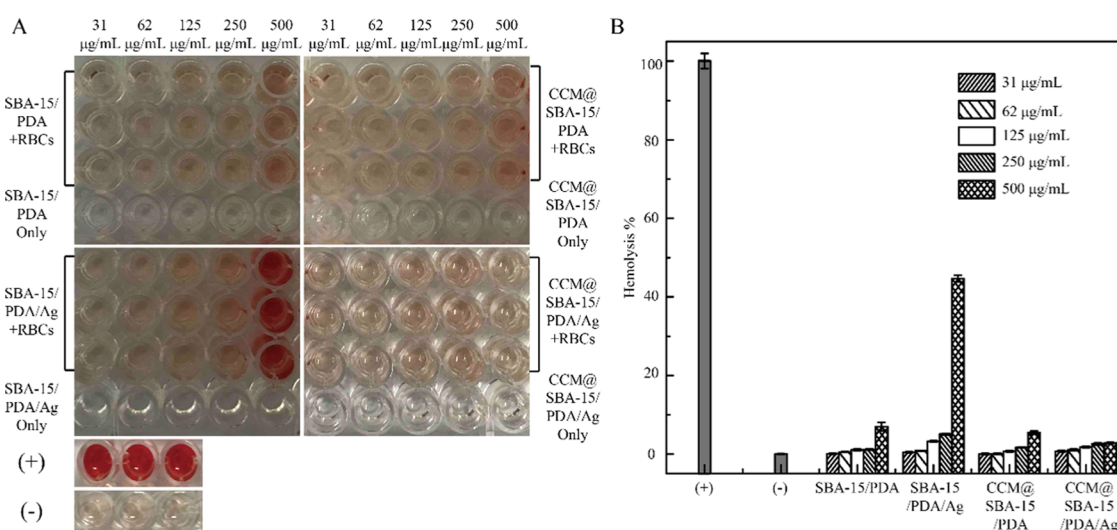
Figure 2. (A) Hemolytic assay images and (B) hemolysis (%) of nanoexcipient and curcumin-loaded nanoexcipient samples (SBA-15/PDA, SBA-15/PDA/Ag, CCM@SBA-15/PDA, and CCM@SBA-15/PDA/Ag) at different concentrations. RBCs were incubated with different samples at the predetermined concentration at 37 °C for 1 h, and the mixture was centrifuged to detect the cell-free hemoglobin in the supernatant. RBCs incubated with PBS and 0.1% (v/v) Triton X-100 in PBS buffer were used as negative (−) and positive (+) controls, respectively. Values were the average of three independent experiments in triplicate, and error bars were derived thereof ($n = 3$).
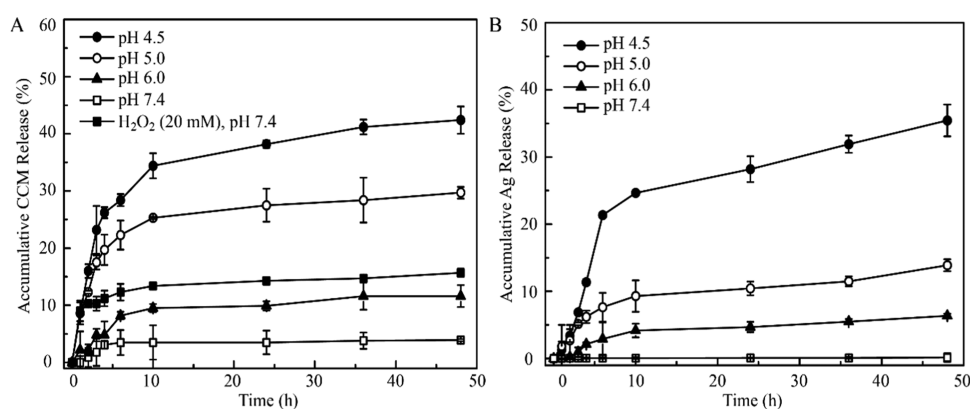
Figure 3. Stimuli-responsive release of the CCM@SBA-15/PDA/Ag composite. (A) pH- and ROS-responsive curcumin release from CCM@SBA-15/PDA/Ag and (B) pH-responsive silver release from CCM@SBA-15/PDA/Ag. Values were the average of three independent experiments in triplicate. Error bars represented standard deviations ($n = 3$).
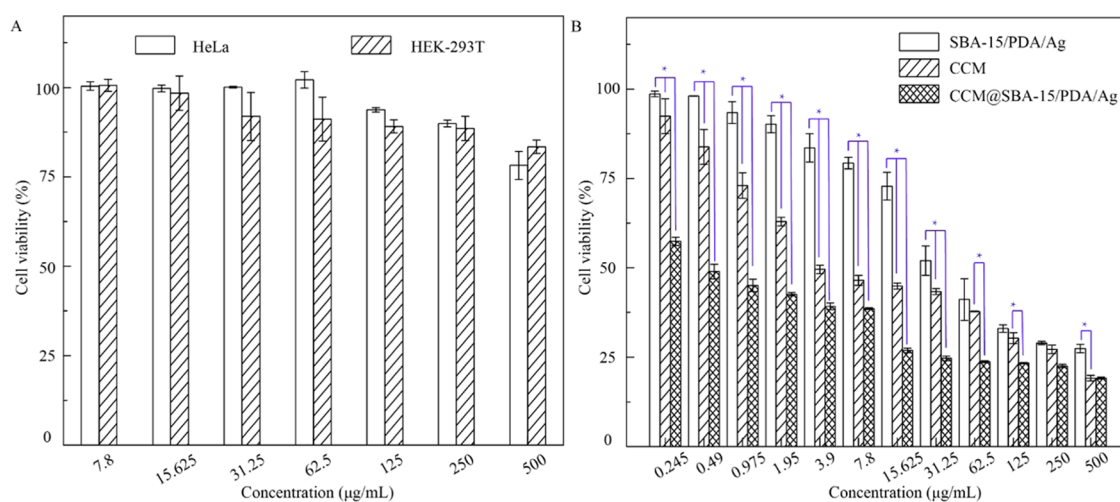

Figure 4. (A) Cytotoxicity assay of HeLa and HEK-293T cell incubation with different concentrations of SBA-15/PDA. (B) In vitro viability of HeLa incubation with different concentrations of SBA-15/PDA/Ag, CCM@SBA-15/PDA/Ag, and free curcumin suspensions for 24 h. Values were the average of three independent experiments in triplicate. Error bars represented standard deviations ($n = 3$). CCM vs SBA-15/PDA/Ag and CCM vs CCM@SBA-15/PDA/Ag at $P < 0.05$ level (*).

hemolytic activity was observed at the concentration of 250 μg/mL. By comparison, further loading curcumin on SBA-15/PDA/Ag composites contributed to a negligible hemolytic activity that occurred even at the highest tested concentration of 500 μg/mL. Therefore, the toxic effect CCM@SBA-15/PDA/Ag on RBCs was significantly lower compared with that of SBA-15/PDA/Ag ($P < 0.05$, there were statistically significant differences between CCM@SBA-15/PDA/Ag- and SBA-15/PDA/Ag-treated groups), which may be attributed to the coordinate bond formation between the carbonyl groups of curcumin and silver[56] to further prevent the release of Ag ions from the mesopores. This observation has revealed the improved biocompatibility to RBCs associated with the loading of phytochemical curcumin in the nanotheranostic excipient in the tested period in comparison with SBA-15/PDA/Ag composites.

2.3. Dual-Stimuli-Responsive Nanocomposites. Targeted drug delivery to lesions of patients has proved an effective therapeutic approach to reduce the harmful side effects of cytotoxic drugs. Among a bunch of constructed stimuli-responsive drug delivery systems, acid- and/or ROS-sensitized nanoexcipients own advantages for targeted delivery of antitumor drugs due to the mildly acidic extra-/intracellular

microenvironment and ROS generation associated with the oxidative stress conditions.[57−59] Due to the presence of PDA in the obtained composite materials, the pH- and ROS-responsive drug release were tested. As shown in Figure 3, both curcumin and silver can be triggered to release from CCM@SBA-15/PDA/Ag composites in a mild acidic condition. When the pH value was 7.4 (physiological conditions), the accumulative release of curcumin was as low as 3.5% within a time period of 48 h. However, at slightly acidic pH 6.0 (mimicking the tumor microenvironment) and pH 4.5 (mimicking the lysosomal condition), an increase of curcumin release, i.e., 11.6% (pH 6.0), 29.7% (pH 5.0), and 42.4% (pH 4.5), at 48 h was observed. Remarkably, the accumulative curcumin release at pH 4.5 was almost 12-fold of that under the neutral condition. Such acid-triggered drug release may be attributed to the protonation of amine groups on the PDA layer and/or on the curcumin molecules, resulting in the destruction of $\pi-\pi$ interactions between PDA and curcumin.

With the addition of 20 mM H_2O_2 in the test solution at a physiological pH of 7.4, an improved release of curcumin was found (Figure 3A). The accumulative curcumin release was determined to be 14.7% after 48 h incubation in the presence of H_2O_2, almost threefold higher than that in the absence of
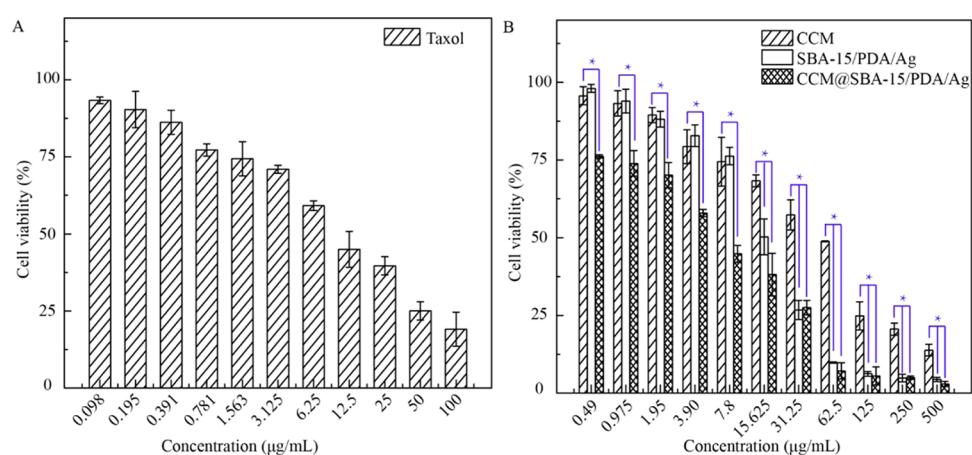
Figure 5. In vitro cytotoxicity assays of A549/TAX cells incubated with different concentrations of (A) free Taxol, (B) SBA-15/PDA/Ag, CCM@SBA-15/PDA/Ag, and free curcumin suspensions for 24 h. Values were the average of measurements in triplicate. Error bars represented as standard deviations ($n = 3$). CCM vs SBA-15/PDA/Ag and CCM vs CCM@SBA-15/PDA/Ag at $P < 0.05$ level (*).
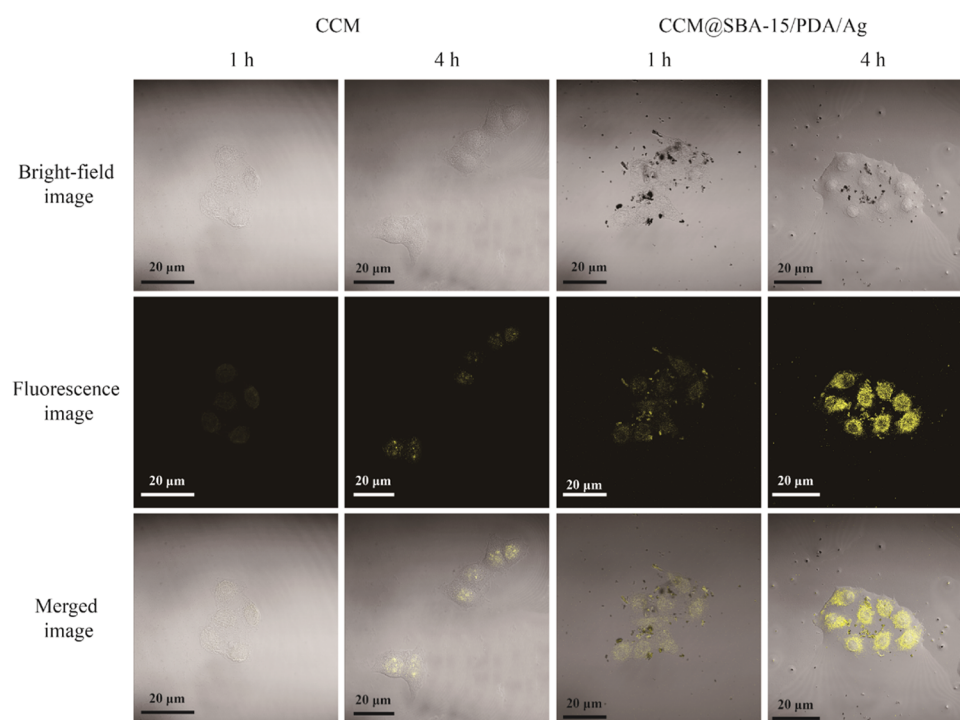

Figure 6. Confocal laser scanning microscopy images of free curcumin and CCM@SBA-15/PDA/Ag composites taken up by HeLa cells at the incubation times of 1 and 4 h.

H_2O_2 (3.5%), possibly due to the breakage of hydrogen bonding between PDA and curcumin through oxidization of the polyphenol groups in the PDA scaffold.[58] Therefore, the sensitive acid- and ROS-responsive curcumin release from the CCM@SBA-15/PDA/Ag composite was successfully achieved. Additionally, the tendency of the pH-triggered release of Ag ions from CCM@SBA-15/PDA/Ag composites was also identified. As shown in Figure 3B, an apparent enhanced accumulative release of silver was determined by ICP-MS with the decreased pH of assay solutions. Besides the pH-affected control release of the PDA layer, this pH-triggered silver release may be attributed to the acid-sensitive nature of silver and/or chelates dissociation. The stimulus including acid and/or ROS in the tumors may facilitate the release of antitumor drugs and silver from SBA-15/PDA nanocarriers and improve

the therapeutic efficacy. Collectively, the sensitive acid- and ROS-responsive attributes identified in obtained CCM@SBA-15/PDA/Ag are desirable for improving its therapeutic efficacy.

2.4. Improved Antitumor Effects of Mesoporous Composites Combined with Curcumin against Drug-Resistant Cancers Cells. As previously reported, phytochemical curcumin as a potent antitumor agent was involved with downregulating and tuning the gene products of the inflammatory transcription factor, nuclear factor-κB activation, and thus was able to induce the apoptosis by p53 and p21 modulation.[17] To test the possible apoptosis induced by obtained materials, the cytotoxicity of SBA-15/PDA was first checked by the standard CCK-8 assay followed by the in vitro assay. SBA-15/PDA of different concentrations ranging from 8
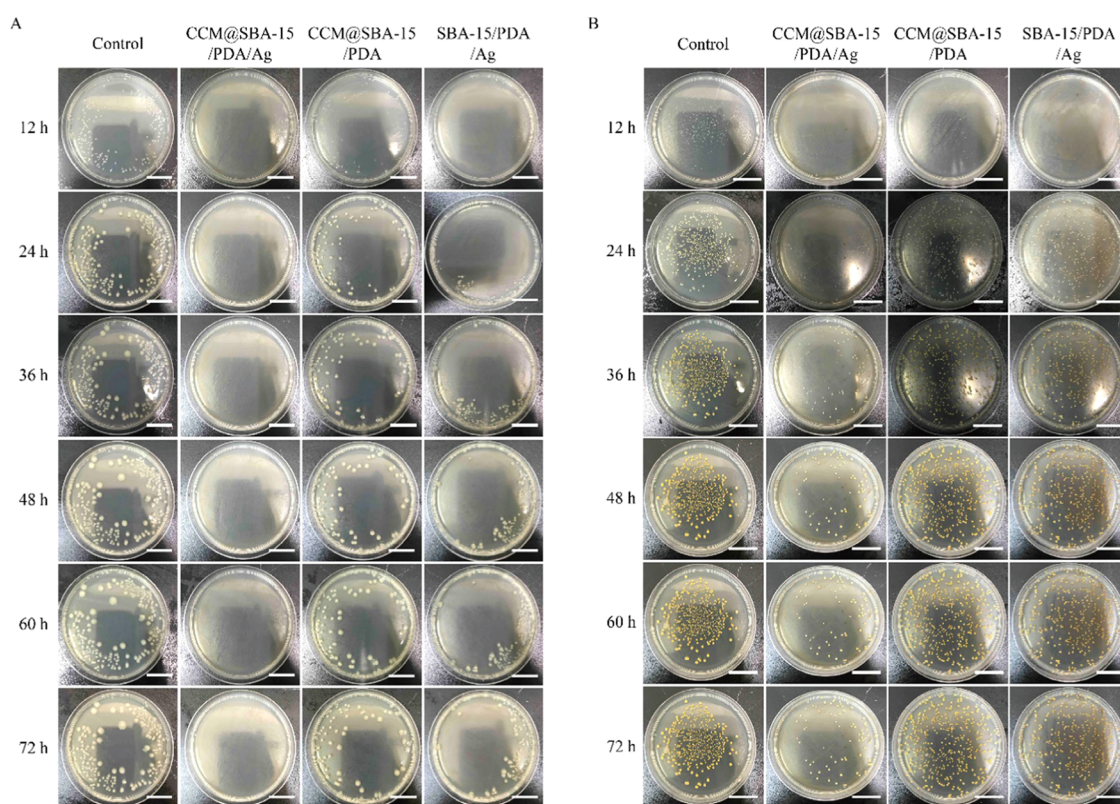
Figure 7. Optical images of agar plates characteristic of the antibacterial activities of SBA-15/PDA, SBA-15/PDA/Ag, CCM@SBA-15/PDA, and CCM@SBA-15/PDA/Ag against *E. coli* (A) and *S. aureus* (B). Assay conditions: 100 μL of 10 mg/mL nanocomposite dispersions were added to the plate with 10 μL of *E. coli* inoculated ($\sim$10^5 cfu/mL); 200 μL of 10 mg/mL nanocomposite dispersions were added to the plate with 10 μL of *S. aureus* inoculated ($\sim$10^5 CFU/mL). Scale bar: 20 mm.

to 500 μg/mL was incubated with malignant HeLa and nonmalignant HEK-293T cells for 24 h, respectively. The results shown in Figure 4A suggested that there was no obvious cytotoxicity for SBA-15/PDA at a concentration as high as 500 μg/mL both for HeLa and HEK-293T cells, indicating good biocompatibility. After the in situ formation of silver nanoparticles on mesoporous SBA-15/PDA, the obvious growth inhibition on HeLa cells was observed (Figure 4B) and the IC$_{50}$ value (half maximal inhibitory concentration of obtained materials) of SBA-15/PDA/Ag was found to be 51.34 μg/mL. Compared with free curcumin, the IC$_{50}$ value of the CCM@SBA-15/PDA/Ag composite was 1.38 μg/mL ([curcumin] = 0.026 μg/mL), whereas the IC$_{50}$ value of free curcumin was 10.99 μg/mL. This enhanced antitumor effect of curcumin after loading on carriers may be attributed to the superior antiproliferative activity of chelated curcumin as well as the synergistic antitumor effect of curcumin and silver, which may be attributed to the induced ROS generation of silver nanoparticles to cause cellular apoptosis.[60] The improved antitumor activity of phytochemical/silver-encapsulated mesoporous composites may help to tackle the drug resistance of cancer cells. Therefore, we measured the cytotoxicity of CCM@SBA-15/PDA/Ag on Taxol-resistant nonsmall cell lung cells (A549/TAX) by the CCK-8 assay. As shown in Figure 5, the obtained IC$_{50}$ value of SBA-15/PDA/Ag was 14.69 μg/mL, while that of the CCM@SBA-15/PDA/Ag composite was 5.05 μg/mL ([curcumin] = 0.095 μg/mL), which was $\sim$8-fold lower than that of free curcumin (IC$_{50}$ = 39.52 μg/mL) and twofold lower than that of free Taxol (IC$_{50}$ = 9.77 μg/mL). Note that the IC$_{50}$ value obtained for CCM@SBA-15/PDA/

Ag is comparable with that of 4-hydroxyemodin (HEM) against A549/TAX (IC$_{50}$ = 2.83 μg/mL).[61] The cytotoxicity of AgNO$_3$ on HeLa and A549/TAX cells was also evaluated by CCK-8 assays (Figure S4), and the IC$_{50}$ values are recorded in Tabel S1. The combination indexes were calculated to be 0.201 and 0.330, respectively, suggesting a synergistic effect of silver and curcumin in CCM@SBA-15/PDA/Ag against HeLa and A549/TAX cells. These observations may suggest the attributing role of the mesoporous composite of CCM@SBA-15/PDA/Ag as an alternative to overcome drug resistance in cancer cells. Moreover, the improved bioavailability of active components of curcumin in the nanocomposite with enhanced cellular internalization may be also beneficial for such an improved antitumor effect of curcumin loading on SBA-15/PDA/Ag. To test this hypothesis, endocytosis and intracellular release of curcumin were monitored using confocal microscopy. The HeLa cells were incubated with free fluorescent curcumin and CCM@SBA-15/PDA/Ag (equal amount of curcumin) for a different time period, respectively. As shown in Figure 6, the curcumin was evidently taken in by HeLa cells and the amount of curcumin in the cells increased with a relatively strong fluorescence observed at a longer incubation time. It should be noted that the incubation of CCM@SBA-15/PDA/Ag composites showed a more visible fluorescence signal than that of free curcumin, which revealed the enhanced intracellular uptake and curcumin release from CCM@SBA-15/PDA/Ag as compared to free curcumin. Therefore, curcumin loading SBA-15/PDA/Ag possessed markedly higher cytotoxicity compared with that of free curcumin. Although good in vitro anticancer effects of CCM@SBA-15/PDA/Ag

were identified, further in vivo studies need to be conducted to check its therapeutic potential.

2.5. Enhanced Antibacterial Effects of Nanocomposites. Note that both curcumin and silver nanoparticles exhibited antibacterial activities. Having established the controllable dual drug delivery matrix, the constructed nanotheranostic excipient was thus also tested for antibacterial utilizations. To evaluate antibacterial activities of obtained materials, Gram-negative (G⁻) *E. coli* and Gram-positive (G⁺) *S. aureus* were used as models using a conventional spread plate method on agar plates. As shown in Figure 7A, the presence of CCM@SBA-15/PDA/Ag resulted in almost no visible *E. coli* bacterial colonies within the incubation time of 72 h in contrast to weak antibacterial activities of CCM@SBA-15/PDA and SBA-15/PDA/Ag composites. In the case of *S. aureus*, the antibacterial properties of CCM@SBA-15/PDA/Ag were observed for at least 24 h. By comparison, for CCM@SBA-15/PDA and SBA-15/PDA/Ag composites, the pronounced antimicrobial effects were identified to be as low as 12 h (Figure 7B). The improved antibacterial properties of CCM@SBA-15/PDA/Ag may be attributed to the presence of CCM, enhancing the binding of Ag to the bacterial membrane and generation of more ROS that lead to membrane damage and intracellular content leakage.[62] Based on the observations of Figure 7A,B, the as-prepared CCM@SBA-15/PDA/Ag appeared more effective toward *E. coli* (G⁻) than *S. aureus* (G⁺), possibly due to the altered cellular structure in G⁺ and G⁻ bacteria. For example, the negatively charged lipopolysaccharides (LPS) in the *E. coli* cell wall favored interactions with positively charged silver nanoparticles, which became more vulnerable than *S. aureus*.[63,64] Nevertheless, the as-prepared CCM@SBA-15/PDA/Ag displayed an improved antibacterial activity.

3. CONCLUSIONS

In summary, we have successfully developed a highly biocompatible mesoporous melanin-like PDA nanoexcipient by the coimmobilization of silver nanoparticles and curcumin and tested its antibacterial and antitumor properties. A set of in vitro experiments have demonstrated that the obtained CCM@SBA-15/PDA/Ag could respond to pH and/or ROS stimuli to trigger the curcumin and/or silver release attributing to the blockage of $\pi-\pi$ stacking and/or hydrogen bonding between the PDA layer and curcumin/silver. In addition to the improved biocompatibility, the coformulation of ecofriendly, natural curcumin in the obtained materials was shown to be effective against the growth of G⁻ *E. coli* and G⁺ *S. aureus* as compared with that of SBA-15/PDA/Ag and CCM@SBA-15/PDA. These observations have pinpointed the possible synergistic antibacterial effects of silver nanoparticles and curcumin, while the mesoporous SBA-15 provided a superior delivery matrix of active components to exhibit a prolonged inhibitory effect on the tested bacteria. Notably, a pronounced chemotherapeutic effect on human cervical cancer cells (HeLa) and Taxol-resistant nonsmall cell lung cells (A549/TAX) was also observed when the nanoformulation of curcumin was used compared with that of free curcumin. Taken together, the constructed dual-stimuli-responsive CCM@SBA-15/PDA/Ag composites with desirable biocompatibility and improved chemotherapy and antibacterial activities fulfill diverse demands in dealing with infectious bacteria and drug resistance in cancers and thus hold enormous potentials for biomedical applications.

4. EXPERIMENTAL SECTION

4.1. Materials. Curcumin (CCM), tetraethyl orthosilicate (TEOS), and $AgNO_3$ were obtained from Sinopharm. The mesostructure-directing template of P123 of the triblock copolymer (M_w = 5800, $EO_{20}PO_{70}EO_{20}$) was from Sigma-Aldrich (Germany). Dopamine hydrochloride was bought from Aladdin (Shanghai, China). The stock solution of $AgNO_3$ (0.1005 M) was purchased from NACIS (Qingdao, China). All reagents were used as received, and ultrapure Milli-Q water (resistance > 18 MΩ/cm) was used for the test.

4.2. Synthesis of the Nanoexcipient and Curcumin Loading. In situ synthesis of silver-decorated, polydopamine-coated mesoporous SBA-15 (SBA-15/PDA/Ag) was prepared following our recent report with modifications.[50] First, 80 mL of P123 (0.05 g/mL) was added to 70 mL of HCl (3.4 M) solution. After stirring for 3 h, 9.14 mL of TEOS was added to the solution. Then, after the overnight reaction, the solution was carefully decanted into a Teflon autoclave followed by a heating step of 100 °C for another 24 h. The product was washed and dried. Mesoporous SBA-15 was obtained after calcination at 550 °C for 6 h. To produce SBA-15/PDA, SBA-15 was mixed with dopamine (w/w 5:3) in 10 mM Tris−HCl solution (pH 8.5) via a 24 h ultrasonic bath incubation. After centrifugation, the precipitate was washed three times with ultrapure water and dried. SBA-15/PDA (40 mg) was mixed with $AgNO_3$ (2 mL, 32 mM) at 80 °C in 10 mM Tris−HCl solution (pH 8.5) for 12 h under stirring. The precipitate was washed three times with ultrapure water and dried to obtain the nanoexcipient SBA-15/PDA/Ag. The freshly made nanoexcipient SBA-15/PDA/Ag (100 mg) was mixed with curcumin (2 mg) under stirring in the methanol/DMSO solution at 85 °C to load curcumin via $\pi-\pi$ stacking and/or hydrogen bonding between curcumin and the PDA layer and/or via conjugation with silver.[56,65,66] The resulting curcumin-loaded nanoexcipient (CCM@SBA-15/PDA/Ag) was centrifuged, washed with water and ethanol to remove excessive curcumin, and dried. Similarly, CCM@SBA-15/PDA was prepared using SBA-15/PDA as the nanoexcipient instead of SBA-15/PDA/Ag.

4.3. Characterization. The microscopic features of synthesized materials were observed using a scanning electron microscope (SEM, Hitachi SU-1510, Japan) with an operation voltage of 15 kV and a transmission electron microscope (TEM, JEOL-1010, Japan) operated at 200 kV. Fourier transform infrared (FT-IR) spectra were achieved using a Bruker Fourier spectrophotometer by the KBr pellet technique. The XRD patterns were obtained using a Smartlab TM 9 kW (Rigaku Corporation, Tokyo, Japan) equipped with a rotating anode and Cu Kα radiation (λ = 0.154 nm). The N_2 sorption isotherms were obtained using a Micromeritics ASAP-2020 sorptometer in a conventional volumetric mode. The specific surface area was deduced using the Brunauer−Emmett−Teller (BET) formula. The pore size distribution of synthesized materials was calculated using Barret−Joyner−Halender (BJH) methods. The silver contents of SBA-15/PDA/Ag and CCM@SBA-15/PDA/Ag were determined by an inductively coupled plasma emission spectrometer (ICP, PE Optima 2000DV). The zeta potential values were measured using a Nano-2S90 zetasizer (Malvern, UK).

4.4. Hemolysis Assay. The hemolysis assay was performed as reported with slight modifications.[51] First, fresh rat red blood cells (RBCs) were washed with PBS buffer three times,

and then, the cell pellets were resuspended in PBS buffer to achieve an approximate 4% (v/v) suspension. Afterward, 1.0 mL of RBC suspension was first mixed with equivolume of the nanoexcipient and curcumin-loaded nanoexcipient suspensions of different concentrations followed by 1 h incubation at 37 °C. After centrifuging at 5000 rpm for 5 min, 100 μL of supernatant was transferred to a 96-well plate, of which the absorbance was measured at 570 nm using a Varioskan Flash (Tecan Infinite M200 Pro, Switzerland). Negative and positive controls were prepared using RBC suspensions incubated with PBS and 0.1% (v/v) Triton X-100, respectively. All nano-excipient and curcumin-loaded nanoexcipient samples were measured in triplicate. The percentage of hemolysis was calculated using the following formula: hemolysis (%) = (sample absorbance − absorbance of negative control)/(absorbance of positive control − absorbance of negative control) × 100. A statistical comparison of the percentage of hemolysis of SBA-15/PDA, SBA-15/PDA/Ag, CCM@SBA-15/PDA, and CCM@SBA-15/PDA/Ag was performed using one-way analysis of variance (ANOVA) and Tukey's posthoc multiple comparison test. P values of <0.05 were considered significant. All statistical analyses were performed using GraphPad Prism.

4.5. Stimuli-Responsive Drug Release. To determine the pH- and ROS-triggered drug release kinetics, 5 mg of CCM@SBA-15/PDA/Ag composite was immersed in 2 mL of different buffer solutions and then incubated at 37 °C with shaking at 220 rpm. The pH values of the buffer solutions were 4.5, 5.0, 6.0, and 7.4 for the pH-responsive release. For ROS-responsive drug release, H_2O_2 was added to the PBS solution (pH 7.4) to reach a final concentration of 20 mM. The supernatant (2 mL) was collected at incubation time intervals of 1, 2, 3, 4, 6, 10, 24, 36, 48 h. For each sample taken out, 2 mL of fresh buffer was added into the incubation solution. The concentration of released curcumin was analyzed by HPLC (Shimadzu, Japan), and the released silver amount was determined by inductively coupled plasma mass spectrometry (ICP-MS; Thermo Scientific iCAP Q).

4.6. Cytotoxicity Assay. Human cervical cancer cells (HeLa) and human embryonic kidney cells (HEK-293T) were cultured in Dulbecco's modified Eagle's medium (DMEM, Gibco), while Taxol-resistant human nonsmall cell lung cells (A549/TAX) were cultured in Roswell Park Memorial Institute 1640 Medium (RPMI-1640, Gibco). All of the cell culture media were supplemented with 10% (v/v) fetal bovine serum (FBS, Gibco) and 1% penicillin−streptomycin (Gibco) in a humidified 5% CO_2 atmosphere at 37 °C, and 300 ng/mL Taxol was added in the culture medium for A549/TAX. For the cytotoxicity assay, HeLa, HEK-293T, and A549/TAX cells were seeded into 96-well plates at a density of 4000 cells/well and incubated for 24 h. The cells were then incubated with different concentrations of nanocomposites including SBA-15/PDA, SBA-15/PDA/Ag, CCM@SBA-15/PDA/Ag, and free curcumin, respectively. After 24 h incubation, the suspensions were replaced by 100 μL/well of fresh culture media and 10 μL/well of Cell Counting Kit-8 solution (CCK-8, MedChem Express) was added followed by 2 h incubation. The color intensity of the solution reflecting the cell growth status was measured at 450 nm by a Varioskan Flash. The cytotoxicity of Taxol for A549/TAX cells was also measured to evaluate the drug resistance of the cancer cells. The IC_{50} values were determined to evaluate the cell viability using untreated cells as the control. Additionally, combination analysis of CCM and

Ag was performed based on the calculation of combination indices (CIs), according to the equation CI = $a/A + b/B$, where a is the IC_{50} value of CCM in the form of CCM@SBA-15/PDA/Ag, b is the IC_{50} value of Ag in the form of CCM@SBA-15/PDA/Ag, A is the IC_{50} value of free CCM, and B is the IC_{50} value of Ag ions. Accordingly, if CI < 1 shows synergism, CI = 1 indicates the additive effect and CI > 1 shows antagonism. A statistical comparison of the cell viability using groups treated with SBA-15/PDA/Ag, CCM, and CCM@SBA-15/PDA/Ag was performed using one-way analysis of variance (ANOVA) and Tukey's posthoc multiple comparisons test. P values of <0.05 were considered significant. All statistical analyses were performed using GraphPad Prism.

4.7. Endocytosis and Intracellular Release Assay. HeLa cells (2 mL, 16 000 cells/mL) were plated on the glass bottom dish and cultured for 24 h. The cells were then incubated with 40 μg/mL curcumin and the CCM@SBA-15/PDA/Ag composite for 1 or 4 h. Subsequently, the dish was washed three times with PBS and fixed with methanol. A confocal laser scanning microscope (Zeiss LSM 700, Germany) was used to visualize the distribution of curcumin in cells.

4.8. Antibacterial Assay. All experimental stuffs were sterilized prior to the test. Antibacterial activity was examined based on a spread plate method using *Staphylococcus aureus* (*S. aureus* ATCC 6538) and *Escherichia coli* (*E. coli* ATCC 25922) as models. Typically, 10 μL of *S. aureus* and *E. coli* suspensions (~10^5 CFU/mL) was spread on the agar plates (90 mm in diameter), respectively. To better visualize the antimicrobial activity, the amounts of composites used for the assay were optimized. Therefore, the dispersions of each SBA-15/PDA, SBA-15/PDA/Ag, CCM@SBA-15/PDA, and CCM@SBA-15/PDA/Ag (10 mg/mL) of 100 μL and 200 μL were added to agar plates coated with *S. aureus* and *E. coli* incubated at 37 °C for 12−72 h, respectively. A digital camera was used to record the optical images of incubated plates. Plates for each were prepared in triplicate, and the experiment was repeated three times.

■ ASSOCIATED CONTENT

ⓢ Supporting Information

The Supporting Information is available free of charge at https://pubs.acs.org/doi/10.1021/acsomega.0c00912.

> Figure S1, SEM images, EDS mapping results, and X-ray energy-dispersive spectrometry results; Figure S2, small- and wide-angle XRD patterns; Figure S3, zeta potentials of composites; and Figure S4, cell viability of HeLa and A549/TAX cells with $AgNO_3$ (PDF)

■ AUTHOR INFORMATION

Corresponding Authors

Yuan Wu − *Department of Medical Oncology, Jiangsu Cancer Hospital, Jiangsu Institute of Cancer Research, The Affiliated Cancer Hospital of Nanjing Medical University, Nanjing 210009, China*; Email: wu@njmu.edu.cn

Jin Chen − *Center for Global Health, School of Public Health, The Key Laboratory of Modern Toxicology, Ministry of Education, School of Public Health, and Key Laboratory of Antibody Technique of National Health Commission, Nanjing Medical University, Nanjing 211166, Jiangsu, China;* ⓞ orcid.org/0000-0001-8377-2708; Email: okachen30@gmail.com, jchen@njmu.edu.cn

Authors

Yiyan Song − *Center for Global Health, School of Public Health, Nanjing Medical University, Nanjing 211166, Jiangsu, China; Department of Clinical laboratory, The Fifth People's Hospital of Suzhou, Infectious Disease Hospital Affiliated to Soochow University, Suzhou 215000, China*

Ling Cai − *Center for Global Health, School of Public Health, Nanjing Medical University, Nanjing 211166, Jiangsu, China*

Zhongcheng Tian − *The TCM Hospital of Huaian, 223001 Huaian, China*

Complete contact information is available at:
https://pubs.acs.org/10.1021/acsomega.0c00912

Author Contributions

[#]Y.S. and L.C. contributed equally to this work.

Notes

The authors declare no competing financial interest.

■ REFERENCES

(1) Fischbach, M. A.; Walsh, C. T. Antibiotics for Emerging Pathogens. *Science* **2009**, *325*, 1089−1093.

(2) Worthington, R. J.; Melander, C. Combination approaches to combat multidrug-resistant bacteria. *Trends Biotechnol.* **2013**, *31*, 177−184.

(3) Levy, S. B.; Marshall, B. Antibacterial resistance worldwide: causes, challenges and responses. *Nat. Med.* **2004**, *10*, S122−S129.

(4) Misra, R.; Sahoo, S. K. Coformulation of doxorubicin and curcumin in poly(D,L-lactide-co-glycolide) nanoparticles suppresses the development of multidrug resistance in K562 cells. *Mol. Pharmaceutics* **2011**, *8*, 852−66.

(5) Kabanov, A. V.; Batrakova, E. V.; Alakhov, V. Y. Pluronic((R)) block copolymers for overcoming drug resistance in cancer. *Adv. Drug Delivery Rev.* **2002**, *54*, 759−779.

(6) Naito, S.; Yokomizo, A.; Koga, H. Mechanisms of drug resistance in chemotherapy for urogenital carcinoma. *Int. J. Urol.* **1999**, *6*, 427−439.

(7) Moreno-Aspitia, A.; Perez, E. A. Treatment Options for Breast Cancer Resistant to Anthracycline and Taxane. *Mayo Clin. Proc.* **2009**, *84*, 533−545.

(8) Choi, Y.; Lee, J. E.; Lee, J. H.; Jeong, J. H.; Kim, J. A Biodegradation Study of SBA-15 Microparticles in Simulated Body Fluid and in Vivo. *Langmuir* **2015**, *31*, 6457−6462.

(9) Chang, D.; Gao, Y.; Wang, L.; Liu, G.; Chen, Y.; Wang, T.; Tao, W.; Mei, L.; Huang, L.; Zeng, X. Polydopamine-based surface modification of mesoporous silica nanoparticles as pH-sensitive drug delivery vehicles for cancer therapy. *J. Colloid Interface Sci.* **2016**, *463*, 279−287.

(10) Wang, Z.; Chang, Z.; Lu, M.; Shao, D.; Yue, J.; Yang, D.; Li, M.; Dong, W.-f. Janus Silver/Silica Nanoplatforms for Light-Activated Liver Cancer Chemo/Photothermal Therapy. *ACS Appl. Mater. Interfaces* **2017**, *9*, 30306−30317.

(11) Shao, D.; Li, M. Q.; Wang, Z.; Zheng, X.; Lao, Y. H.; Chang, Z. M.; Zhang, F.; Lu, M. M.; Yue, J.; Hu, H. Z.; Yan, H. Z.; Chen, L.; Dong, W. F.; Leong, K. W. Bioinspired Diselenide-Bridged Mesoporous Silica Nanoparticles for Dual-Responsive Protein Delivery. *Adv. Mater.* **2018**, *30*, No. 1801198.

(12) Anand, P.; Kunnumakkara, A. B.; Newman, R. A.; Aggarwal, B. B. Bioavailability of curcumin: Problems and promises. *Mol. Pharmaceutics* **2007**, *4*, 807−818.

(13) Hatcher, H.; Planalp, R.; Cho, J.; Tortia, F. M.; Torti, S. V. Curcumin: From ancient medicine to current clinical trials. *Cell. Mol. Life Sci.* **2008**, *65*, 1631−1652.

(14) Moghadamtousi, S. Z.; Kadir, H. A.; Hassandarvish, P.; Tajik, H.; Abubakar, S.; Zandi, K. A Review on Antibacterial, Antiviral, and Antifungal Activity of Curcumin. *BioMed Res. Int.* **2014**, No. 186864.

(15) Yang, X. X.; Li, C. M.; Huang, C. Z. Curcumin modified silver nanoparticles for highly efficient inhibition of respiratory syncytial virus infection. *Nanoscale* **2016**, *8*, 3040−8.

(16) Zhang, Q.; Polyakov, N. E.; Chistyachenko, Y. S.; Khvostov, M. V.; Frolova, T. S.; Tolstikova, T. G.; Dushkin, A. V.; Su, W. Preparation of curcumin self-micelle solid dispersion with enhanced bioavailability and cytotoxic activity by mechanochemistry. *Drug Delivery* **2018**, *25*, 198−209.

(17) Aggarwal, B. B.; Kumar, A.; Bharti, A. C. Anticancer potential of curcumin: Preclinical and clinical studies. *Anticancer Res.* **2003**, *23*, 363−398.

(18) Kunnumakkara, A. B.; Anand, P.; Aggarwal, B. B. Curcumin inhibits proliferation, invasion, angiogenesis and metastasis of different cancers through interaction with multiple cell signaling proteins. *Cancer Lett.* **2008**, *269*, 199−225.

(19) Sivanantham, B.; Sethuraman, S.; Krishnan, U. M. Combinatorial Effects of Curcumin with an Anti-Neoplastic Agent on Head and Neck Squamous Cell Carcinoma Through the Regulation of EGFR-ERK1/2 and Apoptotic Signaling Pathways. *ACS Comb. Sci.* **2016**, *18*, 22−35.

(20) Govindaraju, S.; Rengaraj, A.; Arivazhagan, R.; Huh, Y. S.; Yun, K. Curcumin-Conjugated Gold Clusters for Bioimaging and Anticancer Applications. *Bioconjugate Chem.* **2018**, *29*, 363−370.

(21) Wang, A.; Muhammad, F.; Qi, W.; Wang, N.; Chen, L.; Zhu, G. Acid-induced release of curcumin from calcium containing nanotheranostic excipient. *ACS Appl. Mater. Interfaces* **2014**, *6*, 14377−83.

(22) Black, K. C. L.; Sileika, T. S.; Yi, J.; Zhang, R.; Rivera, J. G.; Messersmith, P. B. Bacterial Killing by Light-Triggered Release of Silver from Biomimetic Metal Nanorods. *Small* **2014**, *10*, 169−178.

(23) Watts, K. P.; Fairchild, R. G.; Slatkin, D. N.; Greenberg, D.; Packer, S.; Atkins, H. L.; Hannon, S. J. Melanin content of hamster tissues, human tissues, and various melanomas. *Cancer Res.* **1981**, *41*, 467−72.

(24) Schanze, K. S.; Lee, H.; Messersmith, P. B. Ten Years of Polydopamine: Current Status and Future Directions. *ACS Appl. Mater. Interfaces* **2018**, *10*, 7521−7522.

(25) Liu, Y.; Ai, K.; Lu, L. Polydopamine and Its Derivative Materials: Synthesis and Promising Applications in Energy, Environmental, and Biomedical Fields. *Chem. Rev.* **2014**, *114*, 5057−5115.

(26) Liu, S.; Pan, J.; Liu, J.; Ma, Y.; Qiu, F.; Mei, L.; Zeng, X.; Pan, G. Dynamically PEGylated and Borate-Coordination-Polymer-Coated Polydopamine Nanoparticles for Synergetic Tumor-Targeted, Chemo-Photothermal Combination Therapy. *Small* **2018**, *14*, No. 1703968.

(27) Bettinger, C. J.; Bruggeman, P. P.; Misra, A.; Borenstein, J. T.; Langer, R. Biocompatibility of biodegradable semiconducting melanin films for nerve tissue engineering. *Biomaterials* **2009**, *30*, 3050−3057.

(28) Lee, H.; Dellatore, S. M.; Miller, W. M.; Messersmith, P. B. Mussel-inspired surface chemistry for multifunctional coatings. *Science* **2007**, *318*, 426−430.

(29) Lee, H.; Rho, J.; Messersmith, P. B. Facile Conjugation of Biomolecules onto Surfaces via Mussel Adhesive Protein Inspired Coatings. *Adv. Mater.* **2009**, *21*, 431.

(30) Tong, Y.; Shao, L.; Li, X.; Lu, J.; Sun, H.; Xiang, S.; Zhang, Z.; Wu, Y.; Wu, X. Adhesive and Stimulus-Responsive Polydopamine-Coated Graphene Oxide System for Pesticide-Loss Control. *J. Agric. Food Chem.* **2018**, *66*, 2616−2622.

(31) Cheng, W.; Liang, C.; Xu, L.; Liu, G.; Gao, N.; Tao, W.; Luo, L.; Zuo, Y.; Wang, X.; Zhang, X.; Zeng, X.; Mei, L. TPGS-Functionalized Polydopamine-Modified Mesoporous Silica as Drug Nanocarriers for Enhanced Lung Cancer Chemotherapy against Multidrug Resistance. *Small* **2017**, *13*, No. 1700623.

(32) Peng, Y.; Nie, J.; Cheng, W.; Liu, G.; Zhu, D.; Zhang, L.; Liang, C.; Mei, L.; Huang, L.; Zeng, X. A multifunctional nanoplatform for cancer chemo-photothermal synergistic therapy and overcoming multidrug resistance. *Biomater. Sci.* **2018**, *6*, 1084−1098.

(33) Zeng, X.; Luo, M.; Liu, G.; Wang, X.; Tao, W.; Lin, Y.; Ji, X.; Nie, L.; Mei, L. Polydopamine-Modified Black Phosphorous Nanocapsule with Enhanced Stability and Photothermal Performance for Tumor Multimodal Treatments. *Adv. Sci.* **2018**, *5*, No. 1800510.

(34) Sileika, T. S.; Kim, H.-D.; Maniak, P.; Messersmith, P. B. Antibacterial Performance of Polydopamine-Modified Polymer Surfaces Containing Passive and Active Components. *ACS Appl. Mater. Interfaces* **2011**, *3*, 4602−4610.

(35) Chen, M.; Zhang, L.; Yang, B.; Gao, M.; Zhang, X. Facile synthesis of terminal-alkyne bioorthogonal molecules for live -cell surface-enhanced Raman scattering imaging through Au-core and silver/dopamine-shell nanotags. *Anal. Bioanal. Chem.* **2018**, *410*, 2203−2210.

(36) Shang, B.; Wang, Y.; Yang, P.; Peng, B.; Deng, Z. Synthesis of superhydrophobic polydopamine-Ag microbowl/nanoparticle array substrates for highly sensitive, durable and reproducible surface-enhanced Raman scattering detection. *Sens. Actuators, B* **2018**, *255*, 995−1005.

(37) Ryu, J. H.; Messersmith, P. B.; Lee, H. Polydopamine Surface Chemistry: A Decade of Discovery. *ACS Appl. Mater. Interfaces* **2018**, *10*, 7523−7540.

(38) Cheng, F.-F.; Zhang, J.-J.; Xu, F.; Hu, L.-H.; Abdel-Halim, E. S.; Zhu, J.-J. pH-Sensitive Polydopamine Nanocapsules for Cell Imaging and Drug Delivery Based on Folate Receptor Targeting. *J. Biomed. Nanotechnol.* **2013**, *9*, 1155−1163.

(39) Rai, M.; Yadav, A.; Gade, A. Silver nanoparticles as a new generation of antimicrobials. *Biotechnol. Adv.* **2009**, *27*, 76−83.

(40) Morones, J. R.; Elechiguerra, J. L.; Camacho, A.; Holt, K.; Kouri, J. B.; Ramirez, J. T.; Yacaman, M. J. The bactericidal effect of silver nanoparticles. *Nanotechnology* **2005**, *16*, 2346−2353.

(41) Rai, M. K.; Deshmukh, S. D.; Ingle, A. P.; Gade, A. K. Silver nanoparticles: the powerful nanoweapon against multidrug-resistant bacteria. *J. Appl. Microbiol.* **2012**, *112*, 841−852.

(42) Jacob, S. J. P.; Prasad, V. L. S.; Sivasankar, S.; Muralidharan, P. Biosynthesis of silver nanoparticles using dried fruit extract of Ficus carica - Screening for its anticancer activity and toxicity in animal models. *Food Chem. Toxicol.* **2017**, *109*, 951−956.

(43) El-Hussein, A.; Hamblin, M. R. ROS generation and DNA damage with photo-inactivation mediated by silver nanoparticles in lung cancer cell line. *Iet Nanobiotechnol.* **2017**, *11*, 173−178.

(44) Huang, K. J.; Wang, L.; Wang, H. B.; Gan, T.; Wu, Y. Y.; Li, J.; Liu, Y. M. Electrochemical biosensor based on silver nanoparticles-polydopamine-graphene nanocomposite for sensitive determination of adenine and guanine. *Talanta* **2013**, *114*, 43−48.

(45) Tang, L.; Livi, K. J. T.; Chen, K. L. Polysulfone Membranes Modified with Bioinspired Polydopamine and Silver Nanoparticles Formed in Situ To Mitigate Biofouling. *Environ. Sci. Technol. Lett.* **2015**, *2*, 59−65.

(46) Kumar, P.; Govindaraju, M.; Senthamilselvi, S.; Premkumar, K. Photocatalytic degradation of methyl orange dye using silver (Ag) nanoparticles synthesized from Ulva lactuca. *Colloids Surf., B* **2013**, *103*, 658−661.

(47) El-Rafie, H. M.; El-Rafie, M. H.; Zahran, M. K. Green synthesis of silver nanoparticles using polysaccharides extracted from marine macro algae. *Carbohydr. Polym.* **2013**, *96*, 403−410.

(48) Moulton, M. C.; Braydich-Stolle, L. K.; Nadagouda, M. N.; Kunzelman, S.; Hussain, S. M.; Varma, R. S. Synthesis, characterization and biocompatibility of "green" synthesized silver nanoparticles using tea polyphenols. *Nanoscale* **2010**, *2*, 763−770.

(49) Zhou, J.; Duan, B.; Fang, Z.; Song, J.; Wang, C.; Messersmith, P. B.; Duan, H. Interfacial Assembly of Mussel-Inspired Au@Ag@ Polydopamine Core-Shell Nanoparticles for Recyclable Nanocatalysts. *Adv. Mater.* **2014**, *26*, 701−705.

(50) Song, Y.; Jiang, H.; Wang, B.; Kong, Y.; Chen, J. Silver-Incorporated Mussel-Inspired Polydopamine Coatings on Mesoporous Silica as an Efficient Nanocatalyst and Antimicrobial Agent. *ACS Appl. Mater. Interfaces* **2018**, *10*, 1792−1801.

(51) Coady, D. J.; Ong, Z. Y.; Lee, P. S.; Venkataraman, S.; Chin, W.; Engler, A. C.; Yang, Y. Y.; Hedrick, J. L. Enhancement of Cationic Antimicrobial Materials via Cholesterol Incorporation. *Adv. Healthcare Mater.* **2014**, *3*, 882−889.

(52) Song, Y.; Jiang, H.; Shi, X.; Chen, J.; Wu, Y.; Wei, W. Detection of Lead Using a Sensitive Anodic Stripping Voltammetric Method Based on Composite Mesoporous Silica/Bismuth Oxychloride Modified Electrode. *ChemistrySelect* **2018**, *3*, 2423−2429.

(53) Park, J.-h.; Park, J.-k.; Shin, H.-y. The preparation of Ag/ mesoporous silica by direct silver reduction and Ag/functionalized mesoporous silica by in situ formation of adsorbed silver. *Mater. Lett.* **2007**, *61*, 156−159.

(54) Song, Y.; Jiang, H.; Bi, H.; Zhong, G.; Chen, J.; Wu, Y.; Wei, W. Multifunctional Bismuth Oxychloride/Mesoporous Silica Composites for Photocatalysis, Antibacterial Test, and Simultaneous Stripping Analysis of Heavy Metals. *ACS Omega* **2018**, *3*, 973−981.

(55) Smilgies, D.-M. Scherrer grain-size analysis adapted to grazing-incidence scattering with area detectors. *J. Appl. Crystallogr.* **2009**, *42*, 1030−1034.

(56) El Khoury, E.; Abiad, M.; Kassaify, Z. G.; Patra, D. Green synthesis of curcumin conjugated nanosilver for the applications in nucleic acid sensing and anti-bacterial activity. *Colloids Surf., B* **2015**, *127*, 274−280.

(57) Bi, D.; Zhao, L.; Yu, R.; Li, H.; Guo, Y.; Wang, X.; Han, M. Surface modification of doxorubicin-loaded nanoparticles based on polydopamine with pH-sensitive property for tumor targeting therapy. *Drug Delivery* **2018**, *25*, 564−575.

(58) Wang, X.; Zhang, J.; Wang, Y.; Wang, C.; Xiao, J.; Zhang, Q.; Cheng, Y. Multi-responsive photothermal-chemotherapy with drug-loaded melanin-like nanoparticles for synergetic tumor ablation. *Biomaterials* **2016**, *81*, 114−124.

(59) Wu, Q.; Niu, M.; Chen, X.; Tan, L.; Fu, C.; Ren, X.; Ren, J.; Li, L.; Xu, K.; Zhong, H.; Meng, X. Biocompatible and biodegradable zeolitic imidazolate framework/polydopamine nanocarriers for dual stimulus triggered tumor thermo-chemotherapy. *Biomaterials* **2018**, *162*, 132−143.

(60) Hembram, K. C.; Kumar, R.; Kandha, L.; Parhi, P. K.; Kundu, C. N.; Bindhani, B. K. Therapeutic prospective of plant-induced silver nanoparticles: application as antimicrobial and anticancer agent. *Artif. Cells, Nanomed., Biotechnol.* **2018**, *46*, S38−S51.

(61) Lin, H.; Hu, B. C.; He, X. M.; Mao, J. P.; Wang, Y.; Wang, J.; Zhang, T. T.; Zheng, J.; Peng, Y.; Zhang, F. J. Overcoming Taxol-resistance in A549 cells: A comprehensive strategy of targeting P-gp transporter, AKT/ERK pathways, and cytochrome P450 enzyme CYP1B1 by 4-hydroxyemodin. *Biochem. Pharmacol.* **2020**, *171*, No. 113733.

(62) Song, Z.; Wu, Y.; Wang, H.; Han, H. Synergistic antibacterial effects of curcumin modified silver nanoparticles through ROS-mediated pathways. *Mater. Sci. Eng., C* **2019**, *99*, 255−263.

(63) Ghodake, G.; Lim, S.-R.; Lee, D. S. Casein hydrolytic peptides mediated green synthesis of antibacterial silver nanoparticles. *Colloids Surf., B* **2013**, *108*, 147−151.

(64) Amro, N. A.; Kotra, L. P.; Wadu-Mesthrige, K.; Bulychev, A.; Mobashery, S.; Liu, G. Y. High-resolution atomic force microscopy studies of the Escherichia coli outer membrane: Structural basis for permeability. *Langmuir* **2000**, *16*, 2789−2796.

(65) Yu, X.; Tang, X.; He, J.; Yi, X.; Xu, G.; Tian, L.; Zhou, R.; Zhang, C.; Yang, K. Polydopamine Nanoparticle as a Multifunctional Nanocarrier for Combined Radiophotodynamic Therapy of Cancer. *Part. Part. Syst. Charact.* **2017**, *34*, No. 1600296.

(66) Uthappa, U. T.; Kigga, M.; Sriram, G.; Ajeya, K. V.; Jung, H.-Y.; Neelgund, G. M.; Kurkuri, M. D. Facile green synthetic approach of bio inspired polydopamine coated diatoms as a drug vehicle for controlled drug release and active catalyst for dye degradation. *Microporous Mesoporous Mater.* **2019**, *288*, No. 109572.